*Full Length Article*

JHS(E)

Journal of Hand Surgery
(European Volume)
2019, Vol. 44(5) 479–487

DOI: 10.1177/1753193419830924
journals.sagepub.com/home/jhs


# A four-dimensional-CT study of in vivo scapholunate rotation axes: possible implications for scapholunate ligament reconstruction

**Marieke G.A. de Roo[1,2], Marijn Muurling[3], Johannes G.G. Dobbe[2], Michelle E. Brinkhorst[4], Geert J. Streekstra[2] and Simon D. Strackee[1]**

**Abstract**

Additional fixation of the palmar scapholunate interosseous ligament has been advocated to improve the long-term results of dorsal scapholunate interosseous ligament reconstruction. To investigate the validity of this approach, we determined normal scapholunate motion patterns and calculated the location of the scapholunate rotation axis. We hypothesized that the optimal location of the scapholunate interosseous ligament insertion could be determined from the scapholunate rotation axis. Four-dimensional computerized tomography was used to study the wrist motion in 21 healthy participants. During flexion–extension motions, the scaphoid rotates 38° (SD 0.6°) relative to the lunate; the rotation axis intersects the dorsal ridge of the proximal pole of the scaphoid and the dorsal ridge of the lunate. Minimal scapholunate motion is present during radioulnar deviation. Since the scapholunate rotation axis runs through the dorsal proximal pole of the scaphoid, this is probably the optimal location for attaching the scapholunate ligament during reconstructive surgery.

**Keywords**

Scapholunate, in-vivo kinematics, scapholunate kinematics, dynamic imaging, 4-D imaging, 3-D motion analysis

Date received: 29th October 2018; revised: 21st January 2019; accepted: 22nd January 2019

## Introduction

The scapholunate interosseous ligament (SLIL) connects the scaphoid and lunate in the proximal carpal row. It is a U-shaped ligament, with dorsal, proximal and palmar components between the scaphoid and lunate. Typically, the SLIL ruptures after a fall on an outstretched hand, which leads to pain in wrist extension under mechanical load (Kuo and Wolfe, 2008). Depending on the severity and location of the rupture, the wrist kinematics change, and if left untreated, a scapholunate advanced collapse results (Schmitt et al., 2006). Numerous surgical procedures have been used to restore the SLIL. The most common techniques involve reconstructing the dorsal part of the SLIL (Athlani et al., 2018). However, because of unsatisfactory postoperative results of these procedures and limited information about long-term surgical results, new procedures continue to be reported (Bloom et al., 2003), such as the restoration of only the palmar SLIL or both the dorsal and palmar parts (Alonso-Rasgado et al., 2017; Corella et al.,

[1]Plastic, Reconstructive and Hand Surgery, University of Amsterdam, Amsterdam UMC, The Netherlands
[2]Biomedical Engineering and Physics, University of Amsterdam, Amsterdam UMC, The Netherlands
[3]Department of Biomechanical Engineering, Technical University Delft, Delft, The Netherlands
[4]Department of Plastic, Reconstructive and Hand Surgery, University Medical Center Rotterdam, Rotterdam, The Netherlands

**Corresponding Author:**
Marieke G. A. de Roo, Biomedical Engineering and Physics, University of Amsterdam, Meibergdreef 9, 1105 AZ, Amsterdam, The Netherlands.
Email: m.g.deroo@amc.uva.nl

2013; Dunn and Johnson, 2001; Hyrkas et al., 2008; Marcuzzi et al., 2006).

A better understanding of the biomechanical function of the SLIL is necessary to facilitate decision making for choosing surgical reconstruction procedures and improving consensus. The anatomical features of the scapholunate complex play an important role in the biomechanics of this joint. The dorsal part of the SLIL is described as being thick, tight and short, whereas the palmar part of the SLIL is thin, longer and slacker (Buijze et al., 2011; Kauer, 1986). Wrist extension probably causes tension in the palmar part of the SLIL, and wrist flexion could produce tension in the dorsal part of the SLIL combined with closing of the scapholunate joint gap by traction on the palmar SLIL (Kauer, 1974, 1986). The different morphological features of the scaphoid and lunate also affect the scapholunate motion pattern; the proximal surface of the scaphoid has a smaller radius of curvature than the proximal surface of the lunate and there are different curvatures of their corresponding contact surfaces in the radial fossae. Kauer (1974) hypothesized that because of the stiffer structure of the dorsal SLIL and the morphological properties of the scaphoid and lunate, the axis of rotation of the scaphoid relative to the lunate (i.e. the scapholunate rotation axis) should run through the dorsal part of the scapholunate ligament (Figure 1). Therefore the physiological scapholunate rotation axis should be restored during reconstructive surgery of the SLIL to achieve normal motion in the proximal carpal row. However, the location of this scapholunate rotation axis has not been determined in vivo.

We used advanced four-dimensional computerized tomographic (4-D-CT) imaging techniques to assess the normal scapholunate rotation axes for flexion–extension (FE) and radioulnar deviation (RUD) motions of the wrist, to identify a possible location on the scaphoid surface for insertion of the SLIL.

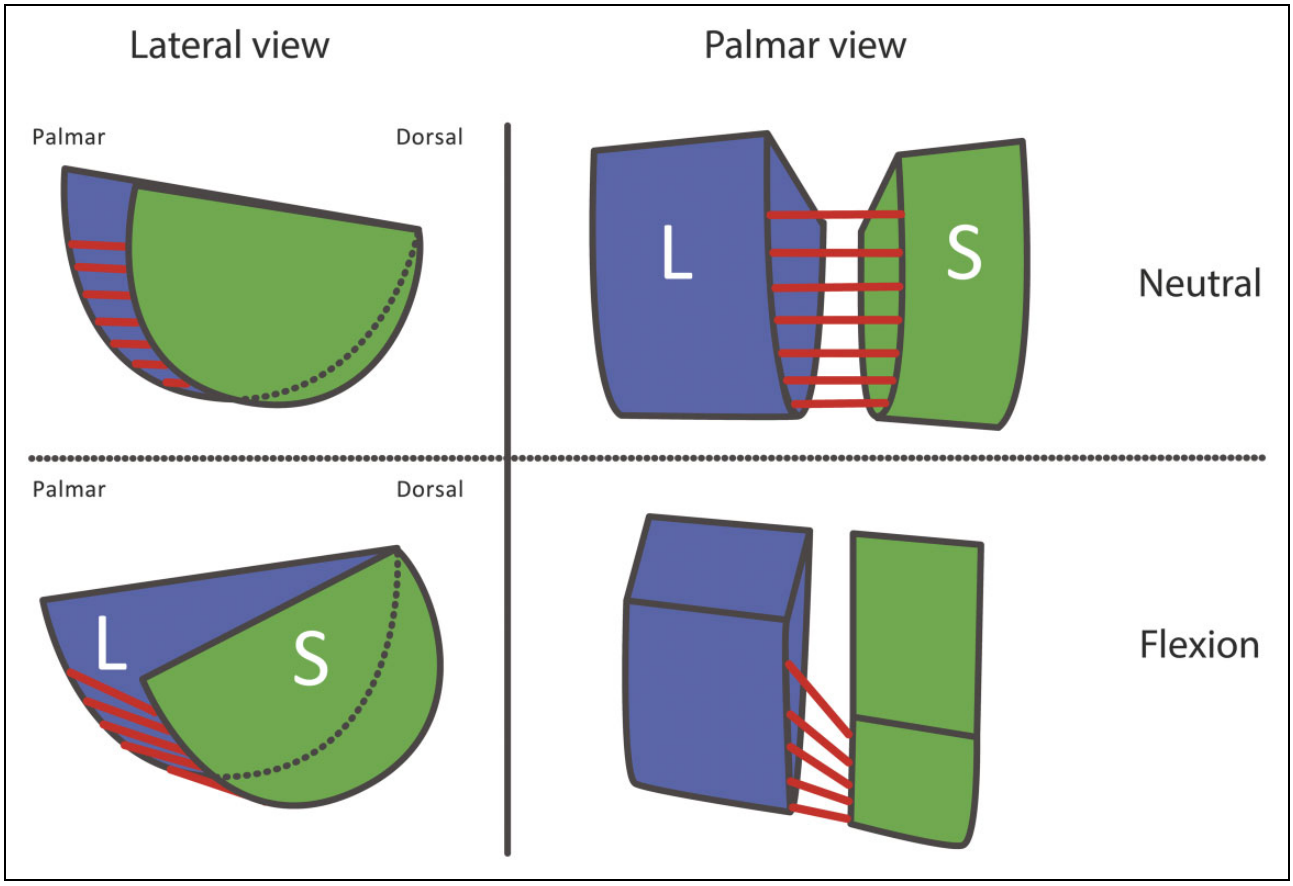


**Figure 1.** According to Kauer (1974), the scaphoid (S; green) shifts proximally with respect to the lunate (L; blue) during wrist flexion due to the different curvatures of the scaphoid and lunate bone surfaces (lateral view). Furthermore, the joint space narrows during wrist flexion caused by the palmar scapholunate interosseous ligament (red lines) visible in the palmar view.

## Methods

### Participants

The participants were in good health and between 20 to 40 years old. Exclusion criteria were previous injuries or disorders of either wrist, pregnancy or being unable to understand the written informed consent. Hypermobility was tested with the Beighton score, and participants in whom hypermobility was present were excluded. Twenty-one participants, aged 21–40 years (11 men, mean age 27 years (range 21–40) and 10 women mean age 28 years (range 21–30)), were included in this study. Information (including the radiation dose) was provided through written information and personal explanation. Informed consent was signed before participation. All study documents and data collection were approved by the Medical Ethics Committee of the Academic Medical Center of Amsterdam.

### Image acquisition

A 64-slice Brilliance CT scanner (Philips Healthcare, Cleveland, OH) was used to acquire three-dimensional CT (3-D-CT) and four-dimensional CT (4-D-CT) scans. During scanning, the participants lay in the prone position with one arm overhead. A 3-D-CT scan of the static wrist in the neutral position was made (120 kV, 75 mAs). The neutral position was clinically defined as the dorsum of the hand being aligned with the longitudinal axis of the radius. 4-D-CT scans of both wrists (120 kV, 30 mAs, 64 slices $\times$ 0.625 mm, axial field of view 4 cm, rotation time 0.4 seconds, scan time 12 seconds) were made during FE motion and RUD motion. The participant moved the wrist actively in 12 seconds from extension to flexion or from radial to ulnar deviation. To keep the wrists within the scanning space, and to allow comparison of motion patterns among participants during the 4-D-CT recording, a custom-made motion device was used in which the fingers enclosed a handgrip (Figure 2). The total dose of the 3-D and 4-D-CT protocol of both wrists was 0.3 mSv.

### Image analysis

All scans of the left wrists were mirrored to right wrists to facilitate identical data analysis. From the static 3-D-CT scan, the scaphoid, lunate, capitate and radius were segmented to yield 3-D polygon models. After segmentation, the outlines of the carpal bones and radius were registered to their representations in each of the corresponding time frames of the 4-D-CT scan to obtain rotation and translation parameters (Dobbe et al., 2018). All image analyses were performed with custom-made software (Dobbe et al., 2011). Validation of the 4-D-CT method used in this trial demonstrated a methodological error in measuring joint kinematics of $<2^\circ$ for rotational and $<1$ mm for translational parameters.

### Determining scapholunate motion patterns

The 3-D-CT scan with the wrist in a static neutral position was used as the FE and RUD angles of $0^\circ$. An anatomical coordinate system of the radius was positioned with a computerized algorithm to compensate for possible differences in the position and

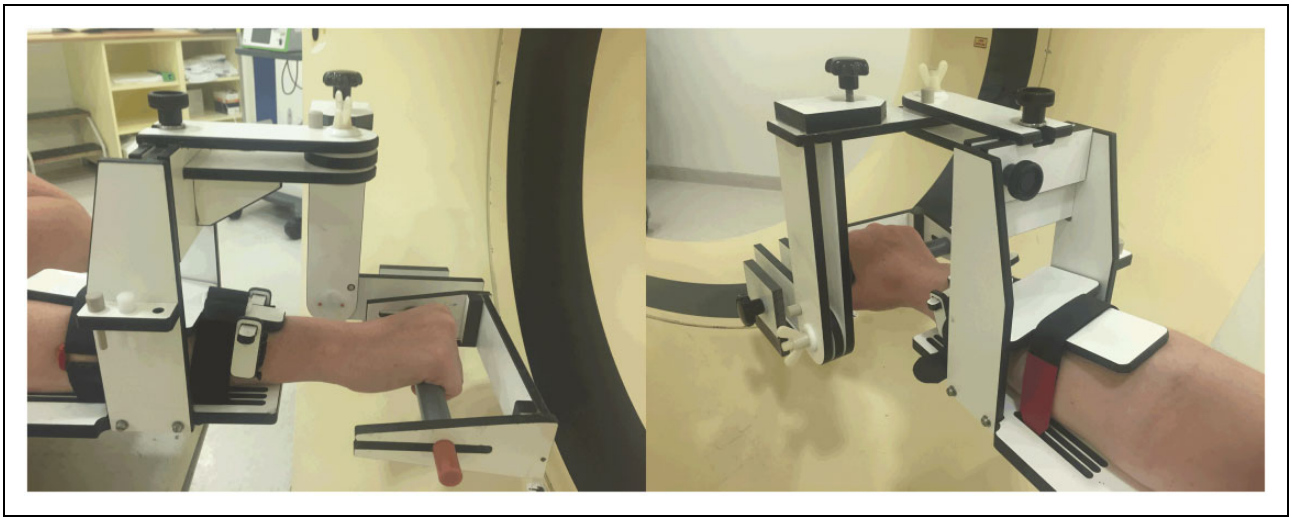

**Figure 2.** Custom made positioning device. The participant lies in the prone position with the wrist extended forward. The positioning device allows active wrist motion along the flexion–extension or radioulnar deviation motion axis. The hand grasps a rod, which can be repositioned to place the wrist in the centre of the two rotation axes of the instrument.

orientation of the radius in the CT-scanner (Kobayashi et al., 1997) (Figure 3). Global wrist motion was defined as the motion of the capitate relative to the radius, expressed in terms of the anatomical coordinate system of the radius. Flexion (X+), extension (X-), radial deviation (Y+), ulnar deviation (Y-), supination (Z+) and pronation (Z-) were defined as rotations of the capitate around the axes of the radial coordinate system. The motion of the scaphoid relative to the lunate was analysed to define the relative rotations and translations during FE and RUD motion. These motion parameters were expressed in terms of the anatomical coordinate system of the radius.

To define the normal scapholunate intercarpal motion patterns for FE and RUD, the mean and 95% confidence intervals (CIs) were calculated for scaphoid and lunate rotation and translation parameters, by linear interpolation for every 5° of motion between 50° extension and 80° flexion, and between 40° ulnar deviation and 40° radial deviation. A linear mixed-effects model was used to check whether gender and hand dominance affected the three translation and three rotation parameters, for both FE and RUD wrist motions. Participants and global wrist motion were included as random effects, and gender and hand dominance as fixed effects. The level of significance was set at $p < 0.05$.

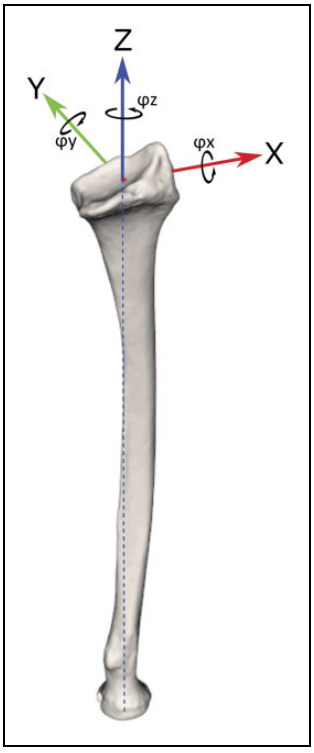


**Figure 3.** Repositioning is expressed in terms of an anatomical coordinate system for the radius. The *Z*-axis (blue) is based on the longitudinal axis of the radius, the *X*-axis (red) points toward the radial styloid, the *Y*-axis (green) is perpendicular to the *X*- and *Z*-axes. The black arrows indicate the rotations around the axes and are referred to as $\phi X$, $\phi Y$ and $\phi Z$ (in degrees). Translations along the axes are referred to as $\Delta X$, $\Delta Y$ and $\Delta Z$ (in millimetres). We define global wrist motion as the motion of the capitate relative to the coordinate system, resulting in flexion (*X*+), extension (*X*-), radial deviation (*Y*+), ulnar deviation (*Y*-), supination (*Z*+) and pronation (*Z*-).

### *Determining the scapholunate rotation axes*

A rotation axis, or the helical axis of motion (Panjabi et al., 1981), was calculated to describe the direction and magnitude of the rotation of the scaphoid with respect to the lunate, when moving from the neutral position of the hand to flexion or extension, or from radial to ulnar deviation. To improve precision in the calculation of the rotation axis, the rotation axes for flexion and extension were determined for five 4-D time frames of the wrist approaching extreme flexion, and five 4-D time frames of the wrist approaching extreme extension. Of these five rotation axes, one mean flexion and extension axis was calculated. This was repeated for RUD motion. To be able to compare the position of the mean rotation axes of differently shaped scaphoids, we selected one single scaphoid as a reference and scaled all the other scaphoids to it. This was done by first determining the size of each scaphoid along its inertial axes and scaling these sizes to the reference scaphoid. The first inertial axis is the axis about which the bone would rotate in a balanced fashion since the weight is closest to the centre of rotation. The remaining two axes are perpendicular to the first (Goldstein, 2001). These scaphoid scaling parameters were applied to the corresponding rotation axes.

To be able to express the variability of the position of the flexion and extension axes in 3-D space among the participants, the mean flexion axis and the mean extension axis of all scaphoid models was first calculated. Then, the uncertainty of each axis location was calculated in the plane perpendicular to the mean axis, represented by a 95% confidence ellipse. These confidence ellipses were determined for every 2 mm equidistantly spaced along each mean axis. Calculation of the 95% confidence ellipses was done using MATLAB (R2017b).

## Results

### *Scapholunate motion patterns*

The data of the scan of one participant during RUD were missing, which resulted in 42 scans with FE

motion and 41 scans with RUD motion. During FE motion, the mean rotation of the scaphoid relative to the lunate around the *X*-axis for 50° of wrist extension was −15° (95% CI: −15.3 to −14.7), to +23° (95% CI: 22.7 to 23.3) for 80° of wrist flexion. Thus, the motion of the scaphoid relative to the lunate during wrist flexion extension is 38° (SD 0.6°) (Figure 4). Rotations around the *Y*- and *Z*-axes were $< 2°$. The translations of the scaphoid relative to the lunate in the *X*-, *Y*- and *Z*-directions were $< 1$, $<3$ and $< 3$ mm respectively. During RUD motion the rotations around the *X*-, *Y*- and *Z*-axes were $< 8°$, $< 2°$, $< 3°$ and the translations in the *X*-, *Y*- and *Z*-direction were $< 1$, $< 2$ and $< 2$ mm respectively (Figure 5). Hand dominance did not significantly affect the patterns of FE and RUD motion. Gender had a significant influence ($p = 0.0016$) on the rotation around the *Y*-axis during FE motion. No significant differences were found in the remaining variables.

### *Rotation axes*

During wrist flexion and extension the rotation axis of the scaphoid relative to the lunate intersected the dorsal ridge of the proximal pole of the scaphoid and was located at the dorsal surface of the lunate (Figure 6). Since the magnitude of the motion of the scaphoid relative to the lunate was $< 8°$ during RUD motion, the variability of the rotation axes were too high to determine a RUD rotation axis reliably.

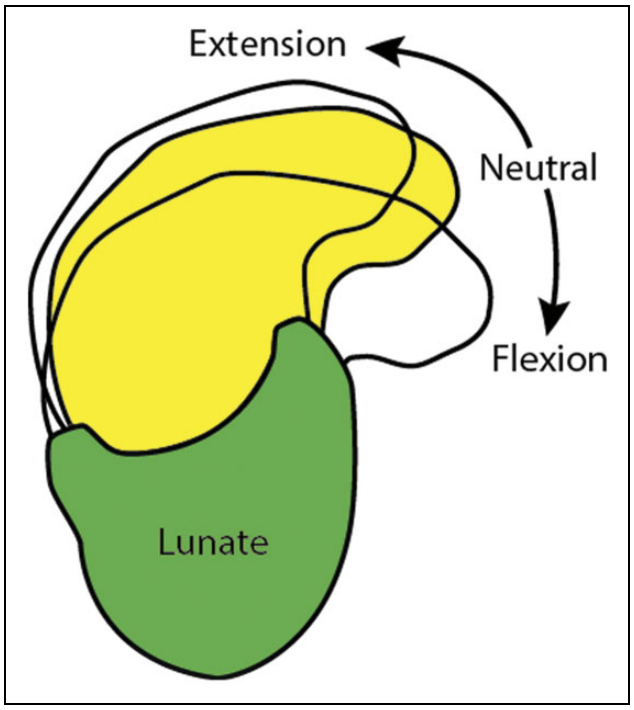


**Figure 4.** Lateral view of the change in position of the scaphoid relative to the lunate (yellow and see-through), with the wrist in 50° extension, neutral and 80° flexion. The scaphoid flexes 38° relative to the lunate between wrist extension and flexion.

## Discussion

The aim of this study was to determine the rotation axis of the scapholunate complex to provide a biomechanical rationale for the optimal point at which to insert the SLIL in reconstructive surgery. The scaphoid was found to rotate 38° (SD 0.6°) relative to the lunate during wrist FE motion. The FE rotation axes intersect the dorsal ridge of the proximal pole of the scaphoid and are located at the dorsal pole of the lunate. Therefore, the dorsal ridge of the scaphoid and dorsal pole of the lunate is considered to be the optimal location for reattachment of the SLIL. Since motion of the scaphoid relative to the lunate was small during RUD motion, a finding also reported by Demehri et al. (2016), only the rotation axes for FE motion were studied.

The large rotation of the scaphoid relative to the lunate around the *X*-axis during FE motion was also described in a study by Wolfe et al. (2000), who quantified this parameter in 20 wrists, with 3-D-CT scans of the wrist in two wrist flexion positions and two wrist extension positions. Our study adds data that provide the dynamic scapholunate motion patterns for every 5° of FE and RUD wrist motion (Figure 5). The results of the normal patterns of motion are in agreement with research done in 3-D in cadavers (Tay et al., 2007; Zhao et al., 2015) and patients (Demehri et al., 2016; Garcia-Elias et al., 2014; Kakar et al., 2016; Wolfe et al., 2000). We found a significant effect of gender on the rotation around the *Y*-axis during FE wrist motion. Since only this variable was significantly different, the difference may be due to the size of the carpal bones rather than gender itself (Rainbow et al., 2008).

There were very small 95% CIs in measurements of FE and RUD wrist motion (Figure 5) indicating that the scapholunate motion patterns in our participant population aged 20 to 40 years were very similar. This was an unexpected finding, since two other studies found that differences in lunate morphology affect carpal kinematics (Abe et al., 2017; Bain et al., 2015). The lunate morphology in the participants in our study consisted of 24 type 1 lunates and 18 type 2 lunates, but lunate morphology did not seem to influence scapholunate kinematics in our study.

The relative scapholunate translations and rotations are expected to be considerably larger in patients with a rupture of the SLIL; Halpenny et al.

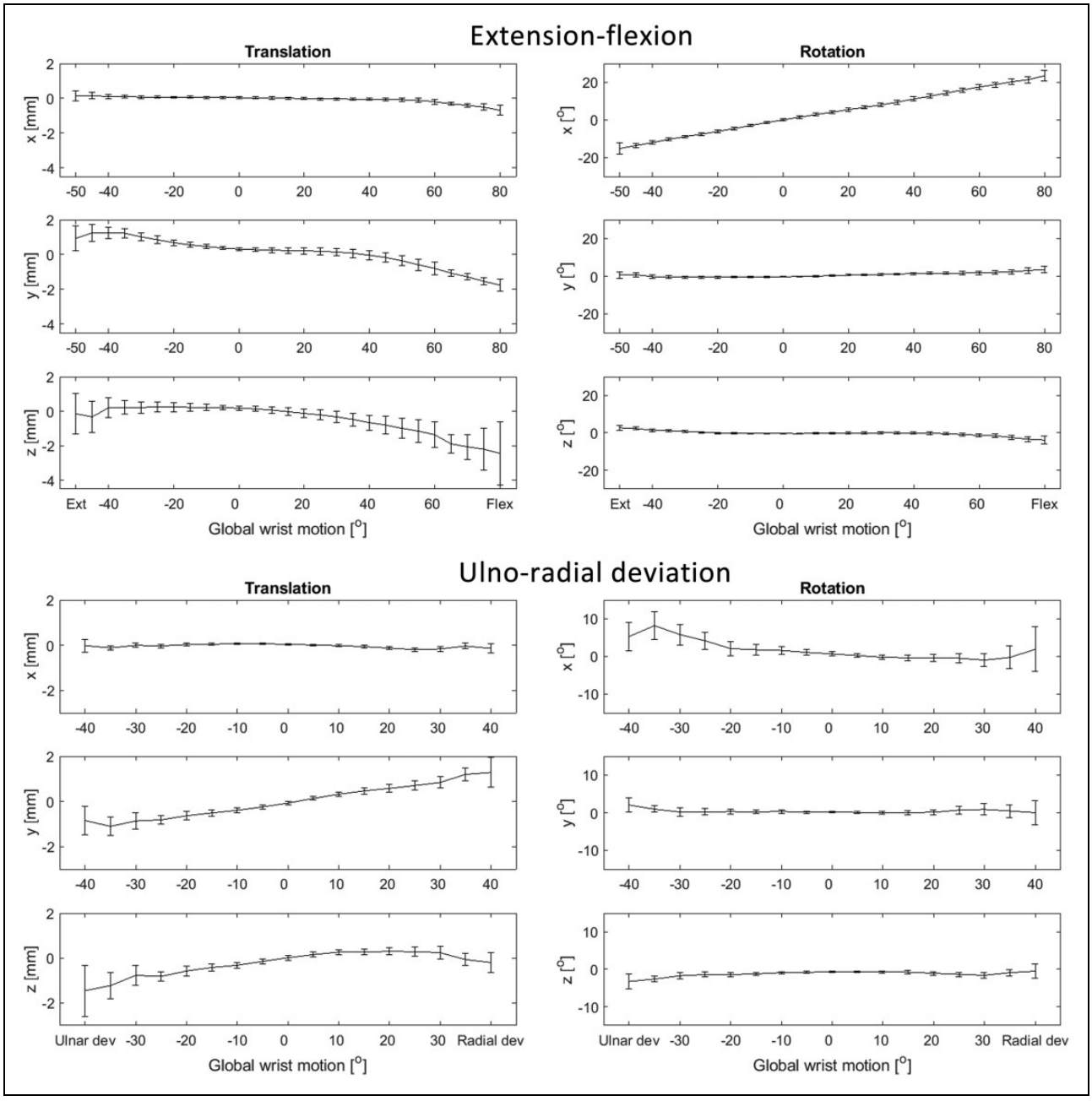


**Figure 5.** The motion of the scaphoid relative to the lunate during wrist extension–flexion and ulnoradial deviation. The horizontal axes show the degree of wrist extension (−), flexion (+), ulnar (−) or radial (+) deviation, which is defined by the rotation of the capitate about the *x*-axis of the anatomical coordinate system (Figure 2). The *y*-axes define the translations (left column) along, and rotations (right column) around the axes of the anatomical coordinate system of the radius. The mean and 95% confidence intervals for every 5° of wrist motion are visualized.

(2012) measured a scapholunate distance of 6 mm. In our results the maximal scapholunate distance was less than 3 mm. The scapholunate motion patterns quantified in this study are potentially useful as a physiological reference in the diagnosis of dynamic SLIL instability.

This study demonstrated that the rotation axes for flexion and extension intersect the scaphoid and lunate on the dorsal surface, confirming the theory of Kauer (1974). This can be explained by the different properties of the dorsal and palmar components of the SLIL, with the dorsal SLIL being tighter and the palmar SLIL being more supple, which affects the position of the rotation point of the scapholunate complex (Kauer, 1974). Separate rotation axes for flexion and extension were therefore calculated for

all 42 wrists to assess whether tension or traction on the palmar or dorsal SLIL from wrist motion would alter the intersection points of the rotation axes. However, both rotation axes intersect the dorsal part of the proximal pole of the scaphoid. The morphology of the proximal surface of the scaphoid and lunate also affects physiological scapholunate motion. The surface of the scaphoid is more curved than the surface of the lunate, and there are different curvatures in their contact surfaces of the radial fossae.

The palmar SLIL has an important role in scapholunate kinematics, for example in closing the scapholunate gap during wrist flexion (Figure 1). However, we believe that it is extremely difficult to precisely restore its function, position and tension during surgery. It is probably only feasible to achieve a taut fixation, which would result in a second non-physiological palmar rotation axis in the scapholunate joint (Figure 6). We expect that taut fixation of the palmar part of the SLIL would hamper the normal 38° of motion between the scaphoid and lunate (Figure 5).

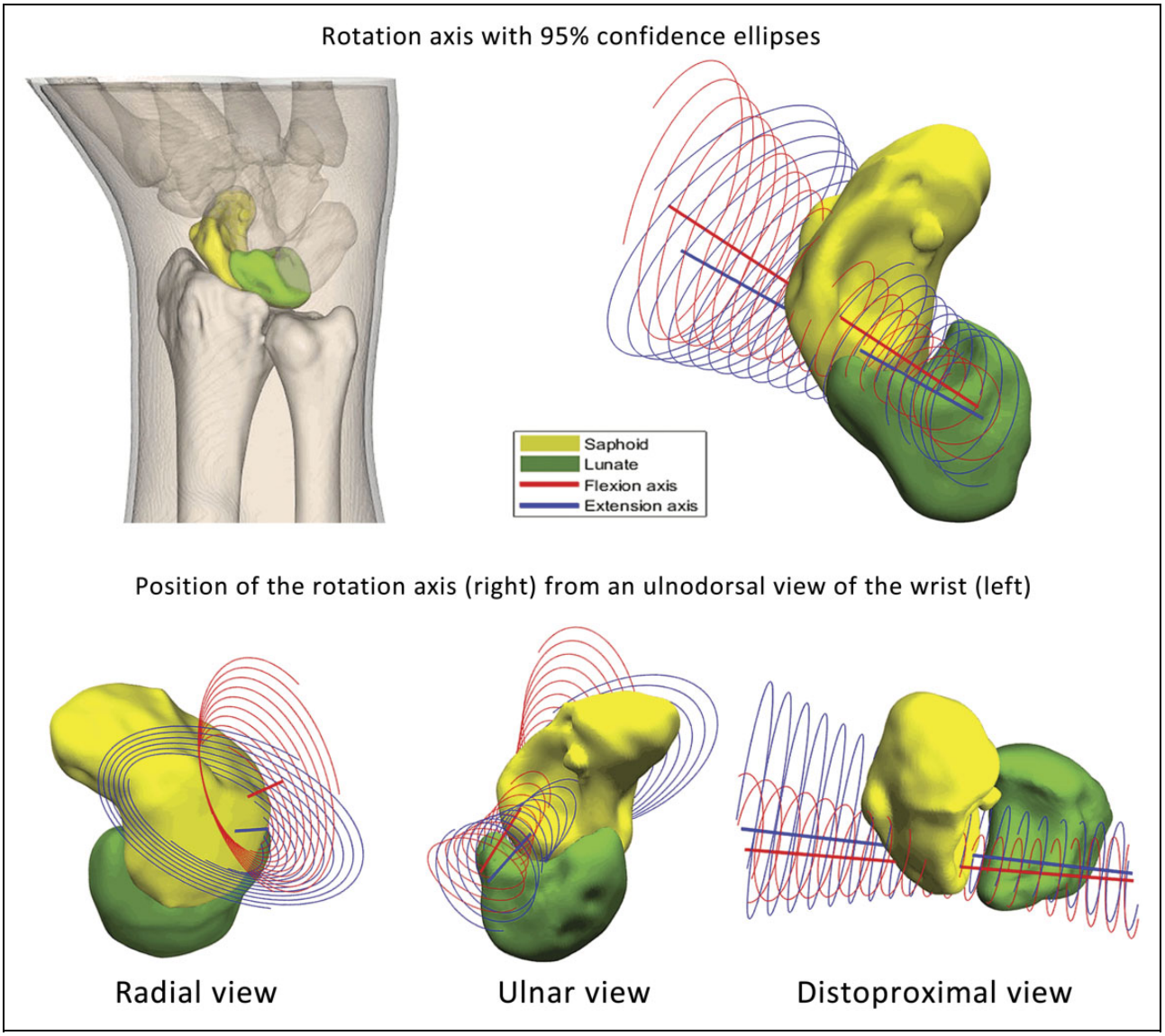


**Figure 6.** The scaphoid rotation axis was determined for all wrists and transformed to one single reference scaphoid (yellow) with its corresponding lunate (green), here shown as a three-dimensional rendering (top row) from an ulnodorsal view of the wrist. The mean flexion rotation axis (red line) and mean extension rotation axis (blue line) and their 95% confidence ellipses are presented. The bottom row shows this configuration and the 95% confidence ellipses in radial, ulnar and distoproximal views.

If a non-physiological position for a new rotation axis is created during reconstruction of the SLIL, we believe that this will limit the natural motion of the scapholunate complex and therefore negatively affects surgical outcomes. Unfortunately, because of heterogeneous reporting of outcome measures in recent and older studies, it remains difficult to compare postoperative outcomes objectively (Alonso-Rasgado et al., 2017; Bloom et al., 2003; Corella et al., 2013; del Piñal et al., 2011; Naqui et al., 2018). Future research on carpal kinematics after dorsal and/or palmar reconstruction of the SLIL should investigate whether the normal pattern of motion of the scapholunate complex can be restored, and investigate which reconstruction significantly increases carpal stability.

Dart-throwing motion is commonly used in daily activities, but it was not studied, since it has been shown that dart-throwing motion occurs predominantly in the midcarpal joint (Moritomo et al., 2014) and SLIL elongation is minimal (Upal et al., 2006). When the SLIL is torn, however, a scapholunate gap was observed by Garcia-Elias et al. (2014), implying that some forces may be applied to the SLIL, which could affect scapholunate motion patterns in the dart-throwing plane of motion. Furthermore, this study did not investigate the effect of axial load on scapholunate motion patterns. Adding an axial load to the carpals, for example by clenching the fist, has been used to identify dynamic instability patterns in patients with an injured wrist (Truong et al., 1994) and is described as changing scapholunate ligament properties (Lee et al., 2010; Scordino et al., 2016; Tan et al., 2018).

**Declaration of conflicting interests** The authors declared no potential conflicts of interest with respect to the research, authorship, and/or publication of this article.

**Ethical approval** Data collection was approved by the Medical Ethics Committee of the Academic Medical Center, University of Amsterdam, Amsterdam. With reference number: 2013_242#C20131578.

**Funding** The authors received no financial support for the research, authorship, and/or publication of this article.

## References

Abe S, Moritomo H, Oka K et al. Three-dimensional kinematics of the lunate, hamate, capitate and triquetrum with type 1 or 2 lunate morphology. J Hand Surg Eur. 2017, 43: 380–6.

Alonso-Rasgado T, Zhang QH, Jimenez-Cruz D et al. Evaluation of the performance of three tenodesis techniques for the treatment of scapholunate instability: flexion–extension and radial-ulnar deviation. Med Biol Eng Comput. 2017, 56: 1091–105.

Athlani L, Pauchard N, Dautel G. Outcomes of scapholunate intercarpal ligamentoplasty for chronic scapholunate dissociation: a prospective study in 26 patients. J Hand Surg Eur. 2018, 43: 700–7.

Bain GI, Clitherow HD, Millar S et al. The effect of lunate morphology on the 3-dimensional kinematics of the carpus. J Hand Surg Am. 2015, 40: 81–9 e1.

Bloom HT, Freeland AE, Bowen V, Mrkonjic L. The treatment of chronic scapholunate dissociation: an evidence-based assessment of the literature. Orthopedics. 2003, 26: 195–203; quiz 4–5.

Buijze GA, Dvinskikh NA, Strackee SD, Streekstra GJ, Blankevoort L. Osseous and ligamentous scaphoid anatomy: Part II. Evaluation of ligament morphology using three-dimensional anatomical imaging. J Hand Surg Am. 2011, 36: 1936–43.

Corella F, Del Cerro M, Ocampos M, Larrainzar-Garijo R. Arthroscopic ligamentoplasty of the dorsal and volar portions of the scapholunate ligament. J Hand Surg Am. 2013, 38: 2466–77.

del Piñal F, Studer A, Thams C, Glasberg A. An all-inside technique for arthroscopic suturing of the volar scapholunate ligament. J Hand Surg Am. 2011, 36: 2044–6.

Demehri S, Hafezi-Nejad N, Morelli JN et al. Scapholunate kinematics of asymptomatic wrists in comparison with symptomatic contralateral wrists using four-dimensional CT examinations: initial clinical experience. Skeletal Radiol. 2016, 45: 437–46.

Dobbe JG, de Roo MG, Visschers JC, Strackee SD, Streekstra GJ. Evaluation of a quantitative method for carpal motion analysis using clinical 3D and 4D CT protocols. IEEE Trans Med Imaging. Epub ahead of print 23 October 2018. DOI: 10.1109/TMI.2018.2877503.

Dobbe JG, Strackee SD, Schreurs AW et al. Computer-assisted planning and navigation for corrective distal radius osteotomy, based on pre- and intraoperative imaging. IEEE Trans Biomed Eng. 2011, 58: 182–90.

Dunn MJ, Johnson C. Static scapholunate dissociation: a new reconstruction technique using a volar and dorsal approach in a cadaver model. J Hand Surg Am. 2001, 26: 749–54.

Garcia-Elias M, Alomar Serrallach X, Monill Serra J. Dart-throwing motion in patients with scapholunate instability: a dynamic four-dimensional computed tomography study. J Hand Surg Eur. 2014, 39: 346–52.

Goldstein H. *Classical mechanics,* 3rd edn. San Francisco, CA, USA, Addison-Wesley, 2001: 191–8.

Halpenny D, Courtney K, Torreggiani WC. Dynamic four-dimensional 320 section CT and carpal bone injury – a description of a novel technique to diagnose scapholunate instability. Clin Radiol. 2012, 67: 185–7.

Hyrkas J, Antti-Poika I, Virkki LM, Ogino D, Konttinen YT. New operative technique for treatment of arthroscopically-confirmed injury to the scapholunate ligament by volar capsuloplasty augmented with a free tendon graft. Scand J Plast Reconstr Surg Hand Surg. 2008, 42: 260–6.

Kakar S, Breighner RE, Leng S et al. The role of dynamic (4D) CT in the detection of scapholunate ligament injury. J Wrist Surg. 2016, 5: 306–10.

Kauer JM. The interdependence of carpal articulation chains. Acta Anat (Basel). 1974, 88: 481–501.

Kauer JM. The mechanism of the carpal joint. Clin Orthop Relat Res. 1986, 202: 16–26.

Kobayashi M, Berger RA, Nagy L et al. Normal kinematics of carpal bones: a three-dimensional analysis of carpal bone motion relative to the radius. J Biomech. 1997, 30: 787–93.

Kuo CE, Wolfe SW. Scapholunate instability: current concepts in diagnosis and management. J Hand Surg Am. 2008, 33: 998–1013.

Lee SK, Park J, Baskies M, Forman R, Yildirim G, Walker P. Differential strain of the axially loaded scapholunate interosseus ligament. J Hand Surg Am. 2010, 35: 245–51.

Marcuzzi A, Leti Acciaro A, Caserta G, Landi A. Ligamentous reconstruction of scapholunate dislocation through a double dorsal and palmar approach. J Hand Surg Br. 2006, 31: 445–9.

MATLAB (R2017b). *Documentation*. Natick, MA: The MathWorks Inc, 2017.

Moritomo H, Apergis EP, Garcia-Elias M, Werner FW, Wolfe SW. International Federation of Societies for Surgery of the Hand 2013 Committee's report on wrist dart-throwing motion. J Hand Surg Am. 2014, 39: 1433–9.

Naqui Z, Khor WS, Mishra A, Lees V, Muir L. The management of chronic non-arthritic scapholunate dissociation: a systematic review. J Hand Surg Eur. 2018, 43: 394–401.

Panjabi MM, Krag MH, Goel VK. A technique for measurement and description of three-dimensional six degree-of-freedom motion of a body joint with an application to the human spine. J Biomech. 1981, 14: 447–60.

Rainbow MJ, Crisco JJ, Moore DC, Wolfe SW. Gender differences in capitate kinematics are eliminated after accounting for variation in carpal size. J Biomech Eng. 2008, 130: 041003.

Schmitt R, Froehner S, Coblenz G, Christopoulos G. Carpal instability. Eur Radiol. 2006, 16: 2161–78.

Scordino L, Werner FW, Harley BJ. Force in the scapholunate interosseous ligament during 2 simulated pushup positions. J Hand Surg Am. 2016, 41: 624–9.

Tan J, Chen J, Mu S, Tang JB, Garcia-Elias M. Length changes in scapholunate interosseous ligament with resisted wrist radial and ulnar inclination. J Hand Surg Am. 2018, 43: 482 e1–e7.

Tay SC, Primak AN, Fletcher JG et al. Four-dimensional computed tomographic imaging in the wrist: proof of feasibility in a cadaveric model. Skeletal Radiol. 2007, 36: 1163–9.

Truong NP, Mann FA, Gilula LA, Kang SW. Wrist instability series: increased yield with clinical-radiologic screening criteria. Radiology. 1994, 192: 481–4.

Upal MA, Crisco JJ, Moore DC, Sonenblum SE, Wolfe SW. In vivo elongation of the palmar and dorsal scapholunate interosseous ligament. J Hand Surg Am. 2006, 31: 1326–32.

Wolfe SW, Neu C, Crisco JJ. In vivo scaphoid, lunate, and capitate kinematics in flexion and in extension. J Hand Surg Am. 2000, 25: 860–9.

Zhao K, Breighner R, Holmes D, Leng S, McCollough C, An KN. A technique for quantifying wrist motion using four-dimensional computed tomography: approach and validation. J Biomech Eng. 2015, 137: 0745011–0745015. DOI: 10.1115/1.4030405.